Magnetic phase diagrams of the antiferromagnetic planar model on a stacked triangular lattice

M. L. Plumer and A. Caillé
Centre de Recherche en Physique du Solide et Département de Physique, Université de Sherbrooke, Sherbrooke, Québec, Canada J1K 2R1
(Received 1 May 1990)

The classical antiferromagnetic planar (XY) model on a simple hexagonal lattice with an applied in-plane magnetic field is studied. With only nearest-neighbor exchange interactions along the c axis, $J_{\parallel} \equiv 1$, and in the basal plane, $J_{\perp}$, the ground-state ($T=0$) phase diagram ($H, J_{\perp}$) exhibits an unexpected richness of ordered states. Finite-temperature effects treated within a molecular-field approximation for a number of values of $J_{\perp}$ reveal complicated (H, T) phase diagrams. Detailed Monte Carlo simulation results are presented for the case of $J_{\perp}=1$ and compared with recent predictions associated with chiral multicritical behavior.

I. INTRODUCTION

Noncolinear magnetic order can arise in simple hexagonal systems of antiferromagnetically coupled ions as a result of frustration imposed by the triangular symmetry of the basal plane.[1] In the case of planar anisotropy, ordering in the basal plane is the so-called 120° spin structure, which can be described as a helically polarized spin density where both the polarization vector **S** and wave vector **Q** lie perpendicular to the c axis. Left- and right-handed ($\pm\mathbf{Q}$) chiral states are degenerate in energy for crystals with a center of inversion symmetry. Kawamura[2-4] has shown that frustrated spin systems of this type are associated with a new kind of universality class ($n=2$ chiral) as characterized by the symmetry of the order parameter $V=Z_2 \times S_1$. Theoretical[2-5] and experimental[3,6-9] estimates of the critical exponents for such chiral spin systems differ significantly from those of the standard xy universality class. Insight into the novel critical behavior of these three-dimensional (3D) systems was gained through earlier studies of the two-dimensional (2D) antiferromagnetic triangular lattice.[10,11]

A magnetic field applied in the basal plane is predicted to split the zero-field transition from paramagnetic to helically ordered phase into two lines of transitions in the (H, T) phase diagram,[12,13] revealing an unusual type of multicritical point at $H=0$, $T=T_N$. Recent neutron diffraction,[8] ultrasonic,[14] and Monte Carlo[15] studies of the quasi-one-dimensional insulator $CsMnBr_3$ confirm the expected convergence of two critical lines at T_N. The detailed analysis of a Landau-type free energy[16] indicates that the two transitions correspond to the following sequence of phases as temperature is decreased: paramagnetic to linear and finally to an elliptically ordered phase. Symmetry, scaling, and renormalization-group arguments[17] suggest that the paramagnetic to linearly polarized phase transition belongs to the of xy (S_1) universality class, the linear to elliptically polarized phase transition belongs to the Ising (Z_2) universality class, and that the multicritical point has critical properties of the $n=2$ chiral universality class. The asymptotic temperature dependence of the critical phase boundaries at T_N is determined by the crossover exponent ϕ, which is estimated for this type of system to be very close to unity ($\phi \cong 1.04$). Similar splitting of the Néel temperature is also observed in mean-field and Monte Carlo results on the 2D triangular lattice,[10,18-20] but with linear and elliptical phases of different symmetries than found in the 3D case for antiferromagnetic coupling along the c axis.

Stimulated by these new results, we investigate here the planar model on a simple hexagonal (stacked-triangular) lattice with nearest-neighbor (NN) antiferromagnetic exchange coupling and an applied in-plane magnetic field. The Hamiltonian can be written as

$$\mathcal{H} = J \sum_{\langle ij \rangle} \mathbf{s}_i \cdot \mathbf{s}_j + J_{\perp} \sum_{\langle kl \rangle} \mathbf{s}_k \cdot \mathbf{s}_l - \sum_i \mathbf{H} \cdot \mathbf{s}_i \ , \tag{1}$$

where $\mathbf{s}_i \perp \hat{\mathbf{c}}$ and $J_{\parallel}, J_{\perp} > 0$ with $\langle i,j \rangle$ and $\langle k,l \rangle$ summed over NN sites along the c axis and in the basal plane, respectively. Except for a special examination of $CsMnBr_3$, we set $J_{\parallel} \equiv 1$ and consider the possible long-range magnetic order stabilized by this system as a function of $J_{\perp}$, magnetic field, and temperature. Exact results at $T=0$ show that four ordered states of different symmetry occur in the ($H, J_{\perp}$) phase diagram, in addition to the 120° spin structure at $H=0$. This serves to extend the previously studied[21] quasi-one-dimensional case $J_{\parallel} \gg J_{\perp}$. The coexistence curves of this phase diagram show quite complicated structure. Finite-temperature effects are treated using a Landau-type expansion of the free energy determined within the molecular-field approximation, and example (H, T) phase diagrams calculated for a number of $J_{\perp}$ values exhibit diverse features. Although this approach is a good approximation to an exact mean-field treatment only in regions close to T_N, it allows the free energy to be expressed as a simple functional of the spin density. Appropriate order parameters are then transparent from a Fourier expansion of the spin density, with the principal component being $\mathbf{Q} = \frac{1}{2}\mathbf{G}_{\parallel} + \frac{1}{3}\mathbf{G}_{\perp}$ (where **G** is a reciprocal lattice vector). Some analytic results are obtained and contact is made with our earlier phenomenological model.[13,16] One of the more unexpected results is for the quasi-two-dimensional case ($J_{\perp} \gg J_{\parallel}$) where the ($H, T$) phase diagram also exhibits splitting of a Néel tem-

perature, but with the linear-elliptical phase boundary being a first-order transition line, thus revealing another novel multicritical point.

In addition to this mean-field analysis, we studied in detail the (H,T) phase diagram near the Néel temperature for the case $J_\perp=1$ by Monte Carlo simulations of a system described by the Hamiltonian (1). The transition at T_N is split as in the quasi-one-dimensional case into two second-order transition lines, allowing tests to be made of the predicted critical behavior. In support of the symmetry, scaling, and renormalization-group analyses, the critical exponent β is estimated to have the values 0.34 ± 0.02 and 0.32 ± 0.02 at the paramagnetic-linear and linear-elliptical phase boundaries, respectively. It is also evident from our data that the crossover exponent ϕ is indeed very close to unity. These results compliment and extend those of Refs. 4 and 15.

II. GROUND-STATE PHASE DIAGRAM

The analysis presented here follows that given in Refs. 22 and 23 for the anisotropic Heisenberg model on a simple hexagonal lattice. With only NN exchange couplings, only three sites on each of two consecutive triangular planes need be considered. Thus, with

$$\mathbf{s}_i=\cos\theta_i\hat{\mathbf{x}}+\sin\theta_i\hat{\mathbf{y}}\ , \tag{2}$$

and $\mathbf{H}\|\hat{\mathbf{x}}$, the ground-state energy, is given by[24]

$$\begin{aligned}E=&\tfrac{1}{3}J_\parallel(\cos\Theta_{14}+\cos\Theta_{25}+\cos\Theta_{36})\\&+\tfrac{1}{2}J_\perp(\cos\Theta_{12}+\cos\Theta_{13}+\cos\Theta_{23}\\&\quad+\cos\Theta_{45}+\cos\Theta_{46}+\cos\Theta_{56})\\&-\tfrac{1}{6}H\sum_i\cos\theta_i\ ,\end{aligned} \tag{3}$$

where $\Theta_{ij}=\theta_i-\theta_j$, $i=1,2,3$, labels sites on one plane and $i=4,5,6$ labels sites on the second plane. The numerical determined $(H,J_\perp)$ phase diagram, with $J_\parallel=1$, is shown in Fig. 1. Following our earlier notation,[13,16] the region labeled 1 is the field-induced ferromagnetic (paramagnetic) state ($\theta_i=0$), phases 5A, 5B, and 5C are denoted as linearly polarized states (see below) and phase 7, the elliptically polarized state. The configurations of the six sublattice spins for the linear and elliptical phases are displayed in Fig. 2 and are distinguished as follows:

phase 5A: $\theta_1=\theta_2=-\theta_4=-\theta_5,\ \theta_3=-\theta_6$,

phase 5B: $\theta_1=-\theta_4,\ \theta_2=-\theta_5,\ \theta_3=-\theta_6$,

phase 5C: $\theta_1=\theta_6=-\theta_3=-\theta_4,\ \theta_2=\theta_5=0$,

phase 7: $\theta_1=-\theta_5,\ \theta_2=-\theta_4,\ \theta_3=-\theta_6$.

Phases 5A and 7 are the ordered states previously discussed in Ref. 21 for the case $J_\parallel\gg J_\perp$. Phases 5B and 5C have apparently not been reported in the literature. Of particular interest regarding Fig. 1 is the result that the state 5B is stable only in a very small region of the phase diagram. The continuous transition from phase 5B to 5C is achieved through a complete alignment with the field direction of one-third of the c axis chains ($\theta_2=\theta_5=0$) and a fanlike configuration describing the remaining spins. A similarly narrow phase region among three linearly polarized states was discovered recently from a phenomenological treatment of spins with strong uniaxial anisotropy of a hexagonal lattice.[25] Further understanding of the phase diagram of fig. 1, and contact made with the results of Ref. 25, follows from an alternate formulation of the ground-state system in terms of a Fourier expansion of the spin density. This description also provides a framework for an analysis of the free energy developed in Sec. III.

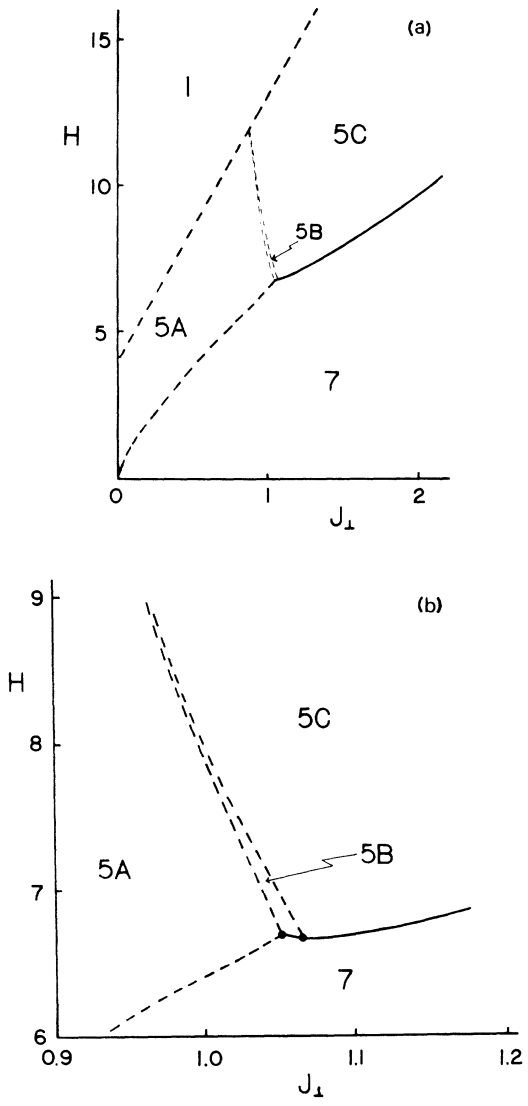

FIG. 1. Ground-state phase diagram with $J_\parallel=1$. Dashed lines denote second-order phase transitions, and the solid line denotes a first-order transition. Regions 1, 5, and 7 represent paramagnetic, linear, and elliptical phases, respectively (see Fig. 2). The 120° spin structure occurs at $H=0$. Details of the phase boundaries near $H\sim6.5$ and $J_\perp\sim1.05$ are shown in (b). H and $J_\perp$ are measured in units of $J_\parallel$.

For this purpose it is convenient to write the ground-state energy from (1) in the general form

$$E=\frac{1}{2V}\int d\mathbf{r}\,d\mathbf{r}'\,J(\mathbf{r}-\mathbf{r}')\mathbf{s}(\mathbf{r})\cdot\mathbf{s}(\mathbf{r}')-\int d\mathbf{r}\,\mathbf{H}\cdot\mathbf{s}(\mathbf{r})\ , \tag{4}$$

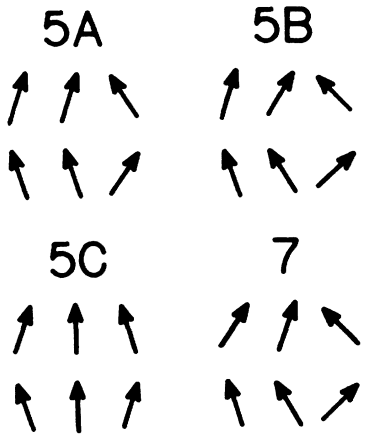

FIG. 2. Schematic representation of the six sublattice magnetization vectors for the linear phases 5 and elliptical phase 7. Shown are two layers of three consecutive basal-plane sites. The magnetic field $\mathbf{H}\|\hat{\mathbf{x}}$ is in the vertical direction.

with the spin density given by[26]

$$\mathbf{s}(\mathbf{r})=\frac{V}{N}\sum_{R}\boldsymbol{\rho}(\mathbf{r})\delta(\mathbf{r}-\mathbf{R}) , \tag{5}$$

where $\mathbf{R}$ denotes hexagonal lattice sites and $\boldsymbol{\rho}(\mathbf{r})$ characterizes the long-range magnetic order. With only NN coupling, the magnetic order can have only a periodicity of 2 (or less) along the c axis and a periodicity of 3 (or less) in the basal plane (i.e., only six sublattice spins are required). The Fourier expansion of $\boldsymbol{\rho}(\mathbf{r})$ can thus be expressed by

$$\boldsymbol{\rho}(\mathbf{r})=\mathbf{m}+\sum_{n=1}^{3}(\mathbf{S}_n e^{i\mathbf{Q}_n\cdot\mathbf{r}}+\mathbf{S}_n^{*}e^{-i\mathbf{Q}_n\cdot\mathbf{r}}) , \tag{6}$$

where the uniform component $\mathbf{m}$ is induced by the applied magnetic field and

$$\mathbf{Q}_1=\tfrac{1}{2}\mathbf{G}_{\|}+\tfrac{1}{3}\mathbf{G}_{\perp},\quad \mathbf{Q}_2=\tfrac{1}{2}\mathbf{G}_{\|},\quad \mathbf{Q}_3=\tfrac{1}{3}\mathbf{G}_{\perp} , \tag{7}$$

e.g., $\mathbf{Q}_1=(\pi/c)\hat{\mathbf{z}}\pm(4\pi/3a)\hat{\mathbf{x}}$. Only the wave-vector component $\mathbf{Q}_3$ has been omitted in our recent studies of magnetic order in hexagonal systems.[13,16,25-27] Equilibrium spin structures are predominantly characterized by the component $\mathbf{Q}_1$, with $\mathbf{S}_1$ being the primary order parameter. The incidental wave-vector components $\mathbf{Q}_2$ and $\mathbf{Q}_3$ are, however, required for a complete description of the magnetic states, serving to distinguish the three linearly polarized phases 5A, 5B, and 5C.

Evaluation of the energy described by (4)–(7) is straightforward, with the result

$$E=J_{\|}(m^2-2S_1^2-2S_2^2+2S_3^2)+3J_{\perp}(m^2-S_1^2+2S_2^2-S_3^2)-mH , \tag{8}$$

where $J_{\|}=(V/N)J(\mathbf{c})$, $J_{\perp}=(V/N)J(\mathbf{a})$, and $S_n^2=\mathbf{S}_n\cdot\mathbf{S}_n^{*}$. Equilibrium states are then determined by minimizing E along with the constraints that $\boldsymbol{\rho}(\mathbf{R}_i)\cdot\boldsymbol{\rho}(\mathbf{R}_i)=1$ for $i=1-6$, the six sublattice sites as described above.

For a description of the ground-state magnetic order, it is convenient to write the polarization vectors as the sum of real and imaginary parts:

$$\mathbf{S}_n=\mathbf{S}_{na}+i\mathbf{S}_{nb} . \tag{9}$$

Note that we can set $\mathbf{S}_{2b}=0$ since $\sin(\mathbf{Q}_2\cdot\mathbf{R})=0$. For a particular choice of phase angles (see below), the phases of Fig. 1 can be characterized by the following *nonzero* Fourier components. Phase 1: m^x, 120° structure: $S_{1a}^y=S_{1b}^x$,

phase 5A: m^x, S_{1a}^y, S_{2a}^y, S_{3a}^x ,

phase 5B: m^x, S_{1a}^y, S_{1b}^y, S_{2a}^y, S_{3a}^x, S_{3b}^x ,

phase 5C: m^x, S_{1b}^y S_{3a}^x ,

phase 7: m^x, S_{1a}^y, S_{1b}^x, S_{2a}^y, S_{3a}^x, S_{3b}^y .

The primary ordering vector in each of the phases 5 is colinear, $\mathbf{S}_1\|\hat{\mathbf{y}}$, describing linearly polarized states. For the elliptical phase, $\mathbf{S}_1$ has an additional component along the field direction (these two components being equal in magnitude for the 120° spin structure at $H=0$). The three phases 5 are distinguished from each other by the relative magnitudes of S_{1a}^y and S_{1b}^y, in addition to the incidental Fourier components. To see this more clearly, let

$$S_{1a}^y=|S_1^y|\cos\phi_1,\quad S_{1b}^y=|S_1^y|\sin\phi_1 . \tag{10}$$

The phase angle ϕ_1 can take values $\phi_1=m\pi/3$ in state 5A, $\phi_1=(2m+1)\pi/6$ in state 5C, and intermediate values in state 5B (i.e., $0<\phi_1<\pi/6$). Note that the incidental component $\mathbf{S}_2$ does not appear in phase 5C. An identical characterization of three linear phases is made in Ref. 25, where the suggestion is made that phases of the type 5B have the symmetry of the three-state Potts model. It can be seen from the above description that a change in spin ordering 7-5B or 7-5C involves a spin flop of $\mathbf{S}_{1b}$ from a configuration $\mathbf{S}_{1b}\|\hat{\mathbf{x}}$ to $\mathbf{S}_{1b}\|\hat{\mathbf{y}}$ so that these transitions are necessarily first order. A phase angle can also be associated with S_3^x for the linear phases:

$$S_{3a}^x=|S_3^x|\cos\phi_3,\quad S_{3b}^x=|S_3^x|\sin\phi_3 , \tag{11}$$

where $\phi_3=m\pi/3$ in both states 5A and 5C. Relationships between the primary and incidental wave-vector components are discussed in Sec. III.

It is straightforward to obtain a few simple analytic results for some of the second-order phase boundaries of Fig. 1. Both 1-5A and 1-5C transitions are given by the same expression,

$$H_{1\text{-}5A}=4J_{\|}+9J_{\perp}=H_{1\text{-}5C} . \tag{12}$$

In the case of strong coupling between triangular planes, $J_{\|}\gg J_{\perp}$, the 5A-7 transition is determined by

$$H_{5A\text{-}7}^2\cong 12J_{\|}J_{\perp} . \tag{13}$$

These results corroborate those of Ref. 21.

III. MOLECULAR-FIELD LANDAU EXPANSION

Within molecular field theory, the Hamiltonian

$$\mathcal{H}=\tfrac{1}{2}\sum_{ij} J_{ij}\mathbf{s}_i\cdot\mathbf{s}_j-\sum_i \mathbf{H}\cdot\mathbf{s}_i \tag{14}$$

is approximated by the variational form

$$\mathcal{H}_{\rm MF}=\sum_i \mathbf{h}_i\cdot\mathbf{s}_i\ , \tag{15}$$

where the effective field $\mathbf{h}_i$ minimizes the free energy ($\delta F/\delta<\mathbf{s}_i>=0$), giving

$$\mathbf{h}_i=\sum_j J_{ij}\langle\mathbf{s}_j\rangle-\mathbf{H}\ . \tag{16}$$

Following a straightforward generalization of the formulation by Bak and von Boehm[28] (also see Ref. 29), a Landau-type expansion of the free energy in powers of $\langle\mathbf{s}_i\rangle$ leads to the following result to sixth order:

$$\begin{aligned}F[\mathbf{s}(\mathbf{r})]=&\tfrac{1}{2}\int d\mathbf{r}\,d\mathbf{r}'\,A(\mathbf{r}-\mathbf{r}')\mathbf{s}(\mathbf{r})\cdot\mathbf{s}(\mathbf{r}')\\&-\int d\mathbf{r}\,\mathbf{H}\cdot\mathbf{s}(\mathbf{r})+\tfrac{1}{4}B\int d\mathbf{r}[\mathbf{s}(\mathbf{r})\cdot\mathbf{s}(\mathbf{r})]^2\\&+\tfrac{1}{6}C\int d\mathbf{r}[\mathbf{s}(\mathbf{r})\cdot\mathbf{s}(\mathbf{r})]^3+\ldots\ ,\end{aligned} \tag{17}$$

where $\langle\mathbf{s}_i\rangle=\mathbf{s}(\mathbf{r})$,

$$A(\mathbf{r})=aT+J(\mathbf{r}),\quad B=bT,\quad C=cT\ , \tag{18}$$

with $a=3$, $b=\frac{9}{5}$, and $c=\frac{297}{175}$ for classical statistics ($S=\infty$). With expressions (5)–(7) and (9) for the spin density, this free energy can be written as a function of $\mathbf{m}$ and the polarization vectors $\mathbf{S}_n$. Magnetic phase diagrams (H,T) are then calculated numerically by minimizing $F(\mathbf{m},\{\mathbf{S}_n\})$ to find equilibrium phases, as characterized in the previous section, for a given set of parameters $(J_\parallel,J_\perp H,T)$.

A few simple analytic results can be obtained from an analysis of the free energy truncated at fourth order and evaluated using only the principal components of the spin density $\mathbf{m}$ and $\mathbf{S}_1$:

$$\begin{aligned}\tilde{F}=&\tfrac{1}{2}A_0'm^2+A_Q S_1^2+BS_1^4+\tfrac{1}{2}B|\mathbf{S}_1\cdot\mathbf{S}_1|^2+\tfrac{1}{4}Bm^4\\&+2B|\mathbf{m}\cdot\mathbf{S}_1|^2+Bm^2S_1^2-\mathbf{m}\cdot\mathbf{H}\ ,\end{aligned} \tag{19}$$

where $\mathbf{m}\|\mathbf{H}\|\hat{\mathbf{x}}$ and

$$A_0'=a(T-T_0'),\quad A_Q=a(T-T_Q)\ , \tag{20}$$

$$T_0'=-(2J_\parallel+6J_\perp)/a,\quad T_Q=(2J_\parallel+3J_\perp)/a\ . \tag{21}$$

The Néel temperature is given by $T_N=T_Q$. A phenomenological version of the above result was recently used by us[16] to study the magnetic phase diagram of $CsMnBr_3$. That work was based on a nonlocal formulation of the free-energy functional[26] where five temperature-dependent fourth-order coefficients $B_p(p=1-5)$ appear [related to the present analysis by $B_p=B(T_N)$], with a, T_0', and T_Q also treated as free parameters. Splitting of the Néel temperature by a magnetic field was shown to be a consequence of competition between the term $|\mathbf{S}_1\cdot\mathbf{S}_1|^2$,

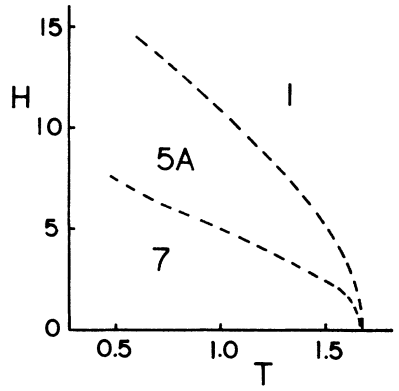

FIG. 3. Phase diagram with $J_\parallel=1$ and $J_\perp=1$ near $T_N=\frac{5}{3}$ calculated using the molecular-field model. Regions 1, 5A, and 7 represent paramagnetic, linear, and elliptical phases, respectively, as characterized in Sec. II. Dashed curves denote lines of second-order transitions.

which stabilizes a helical spin polarization [e.g., $\mathbf{S}_1=S_1(\hat{\mathbf{x}}+i\hat{\mathbf{y}})$ so that $\mathbf{S}_1\cdot\mathbf{S}_1=0$], and the term $|\mathbf{m}\cdot\mathbf{S}_1|^2$, which stabilizes a linear polarization $\mathbf{S}_1\|\hat{\mathbf{y}}$. Expressions for the second-order phase boundaries (see, e.g., Fig. 3) given in Ref. 16 reduce, in the present analysis, and for $T\sim T_N$, to the relations

$$\begin{aligned}H_{1\text{-}5A}^2&\cong-A_Q(\Delta')^2/B(T_N)\ ,\\H_{5A\text{-}7}^2&\cong\tfrac{1}{4}H_{1\text{-}5A}^2\ ,\end{aligned} \tag{22}$$

where $\Delta'=a(T_Q-T_0')$.

In the case of a 2D triangular lattice or a hexagonal lattice with ferromagnetic interplanar coupling, only wave-vector components 0 and $\frac{1}{3}\mathbf{G}_\perp$ contribute to the spin density (6). The free energy in that case contains terms of the form[30] $(\mathbf{m}\cdot\mathbf{S})(\mathbf{S}\cdot\mathbf{S})$, resulting in magnetic phase diagrams with ordered states of different symmetries[10,11] than found here.

Analysis of the full free energy demonstrates the following relationships between the incidental ($\mathbf{S}_2$ and $\mathbf{S}_3$) and primary ($\mathbf{S}_1$) Fourier components of the spin density. To lowest order in $\mathbf{S}_1$, one finds (also see Ref. 27)

$$\mathbf{S}_2+\mathbf{S}_2^*\sim\tfrac{1}{2}\mathbf{S}_1(\mathbf{S}_1\cdot\mathbf{S}_1)+\mathbf{S}_1(\mathbf{m}\cdot S_3^*)+\text{c.c.}\ , \tag{23}$$

$$\mathbf{S}_3\sim\tfrac{1}{2}\mathbf{m}(\mathbf{S}_1\cdot\mathbf{S}_1)+\mathbf{S}_1(\mathbf{m}\cdot\mathbf{S}_1)\ . \tag{24}$$

For linear phases where $\mathbf{S}_1\|\hat{\mathbf{y}}$, the first part of relation (23) yields $S_2\sim S_1^3\cos3\phi_1$, showing that $S_2=0$ in phase 5C [$\phi_1=(2m+1)\pi/6$]. Relation (24) indicates that S_3 is nonzero only if a magnetic field is present; this is a general result valid to all orders. It is evident from these expressions that both S_2 and S_3 are small in regions of the phase diagram of interest here (not too far from T_N) since $S_1^2\sim(T_N-T)$.

Illustrative examples of magnetic phase diagrams calculated from the free energy (17) are shown in Figs. 3, 4, and 5 for $J_\perp=1$, 1.5, and 10, respectively, where $J_\parallel=1$ and with the Néel temperature $T_N=T_Q$ given by (21). In each figure, the 120° spin structure occurs at $H=0$ for

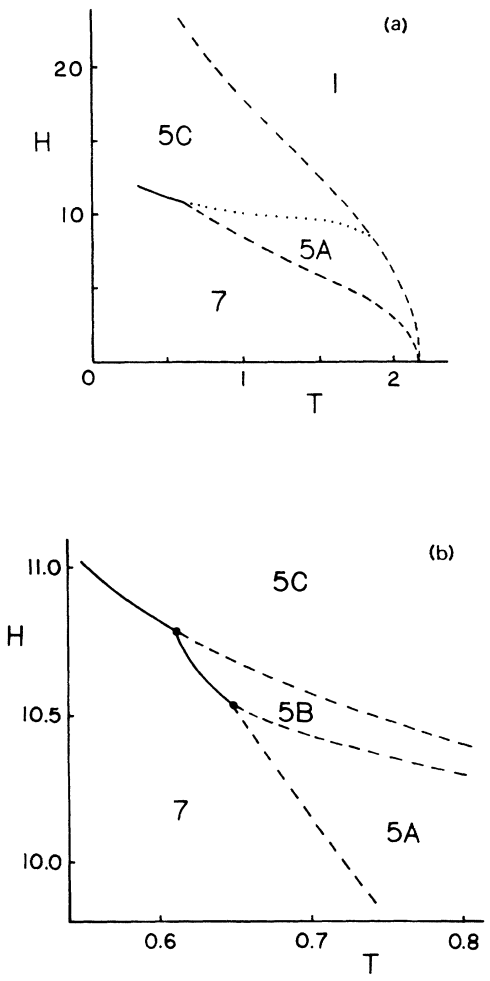

FIG. 4. As in Fig. 3 with $J_\perp = 1.5$ ($T_N = \frac{13}{6}$). Solid curves denote first-order phase boundaries, and the dotted curve represents two second-order boundary lines as shown in (b). The two lines 5A-5B and 5B-5C coalesce at the paramagnetic phase boundary.

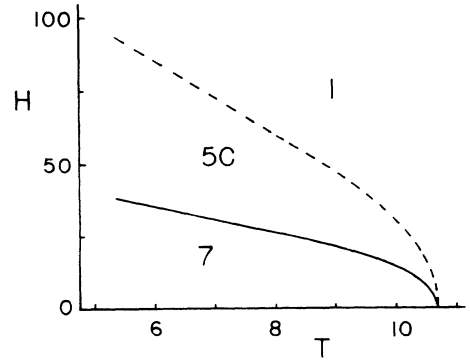

FIG. 5. As in Fig. 3 with $J_\perp = 10$ ($T_N = \frac{32}{3}$). Solid curve represents a first-order transition line.

$T < T_N$. Figure 3 ($J_\perp = 1$) demonstrates the splitting of the Néel temperature by the in-plane field into two lines of second-order phase transitions. The structure of this phase diagram at very low temperatures (outside the range of validity of the present model) must be quite complicated since the sequence of phases $7 \rightarrow 5A \rightarrow 5B \rightarrow 5C \rightarrow 1$ occurs with increasing field strength at $T = 0$ (Fig. 1). An indication of the complexity which can occur is illustrated by Figs. 4(a) and 4(b) ($J_\perp = 1.5$) where all of the phases of Fig. 1 are seen, with the phase 5B again stable only in a very narrow region of the phase diagram, as at $T = 0$. This figure shows a number of unusual types of multicritical points, such as the intersection of four second-order transition lines where phases 1, 5A, 5B, and 5C coalesce. Also note the similarity of Fig. 4(b) and Fig. 1(b). Perhaps more interesting for a wider class of real materials is the phase diagram in the quasi-two-dimensional case ($J_\perp = 10$) shown in Fig. 5 (similar results are also found for $J_\perp = 2$). Splitting of the Néel temperature occurs as in the previous two examples, but here the linear phase has the symmetry of state 5C. A significant, and related, additional difference is that the linear-elliptical phase boundary is a line of first-order transitions. Note, however, that the magnitude of the discontinuity in the order parameters (e.g., S_2^y) across this transition line was found to decrease to zero as $T \rightarrow T_N$. It is not clear that the universality class of the transition at T_N remains $n = 2$ chiral ($V = Z_2 \times S_1$) since the asymptotic merging of Z_2 and S_1 critical lines previously analyzed[17] is absent for this case. The possibility that critical fluctuations drive this transition to be first order at some critical value of $J_\perp$ (not accounted for in the present mean-field treatment) deserves further investigation, especially in view of results by Diep[5] on related systems.

We conclude this section with results for $CsMnBr_3$ calculated as above using the experimentally determined (see, e.g., Ref. 8) exchange parameters $J_\perp = (20.4\ \text{K})S^2$ and $J_\perp = (0.044\ \text{K})S^2$ and with the magnetic field given in physical units (Tesla) determined by $H/(Sg\mu_B)$, where $S = \frac{5}{2}$. T_N calculated from (21) has a value 85.28 K in the present model, to be compared with the experimental result[8,14] of 8.3 K. Such a discrepancy for the Néel temperature in quasi-one-dimensional systems is not surprising in view of results from better calculations which treat only interchain coupling within a mean-field approximation, giving $T_N \sim (J_\parallel J_\perp)^{1/2}$. The phase diagram shown in Fig. 6 has the same general features as found experimentally,[8,14] with Monte Carlo simulations,[15] and our previous phenomenological model.[16] Among notable differences is the very narrow initial splitting of the phase boundaries near T_N. The separation between these transition lines is apparently widened considerably by critical fluctuations as is evident from the Monte Carlo and experimental results. Also note that the 1-5A phase boundary near T_N of Fig. 6 decreases in temperature with increasing field strength, a feature of the isotropic model (Fig. 1) as well. The opposite behavior is observed in the Monte Carlo and experimental results. This feature was accounted for in the phenomenological model of Ref. 16 by assigning a negative value to the coefficient B_5 of the term $m^2 S_1^2$ [see (19)].

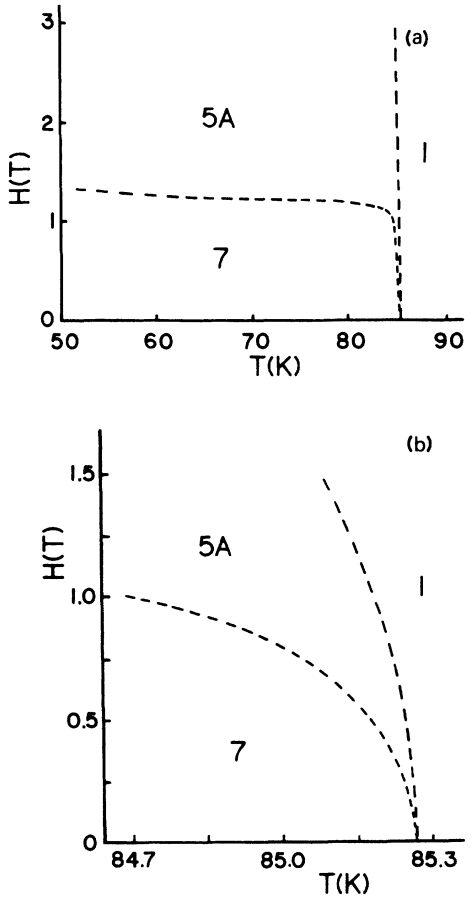

FIG. 6. Phase diagram calculated for quasi-one-dimensional $CsMnBr_3$ with details of the region near T_N shown in (b).

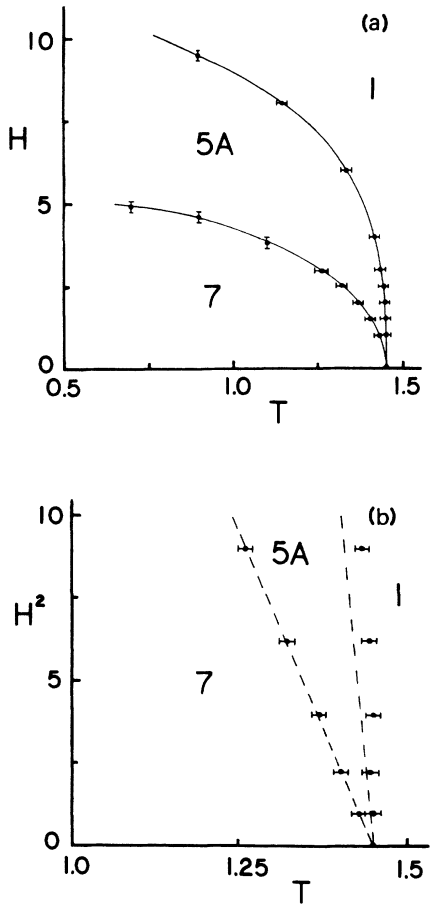

FIG. 7. Phase diagram determined by Monte Carlo simulations with $J_{\parallel}=J_{\perp}=1$. Regions labeled 1, 5A, and 7 represent paramagnetic, linear, and elliptical phases, respectively. Lines in (a) serve as guides to the eye. Linear temperature dependence of H_c^2 for both phase boundaries near $T_N \cong 1.45$ is suggested by the data in (b), where the dashed lines are from the molecular-field relations (22).

IV. MONTE CARLO SIMULATIONS

In order to test predicted critical behavior associated with the splitting of T_N by a field into two second-order transition lines,[17] Monte Carlo simulations of the Hamiltonian (1) with $J_{\parallel}=J_{\perp}=1$ and $\mathbf{H}\|\hat{\mathbf{x}}$ were performed. This investigation serves to extend and compliment the Monte Carlo results of Kawamura,[4] who studied this system with $J_{\parallel}=-1$ and $J_{\perp}=1$ at zero field (the sign of $J_{\parallel}$ should not affect critical behavior at $H=0$) and Mason, Collins, and Gaulin,[15] who studied the magnetic phase diagram of $CsMnBr_3$ using the experimental values for $J_{\parallel}$ and $J_{\perp}$. The standard Metropolis algorithm was employed using periodic boundary conditions on $L\times L\times L$ lattices with $L=12$, 18, and 24. Fourier components of the spin density defined by[31]

$$M_{\alpha}(\mathbf{q})=\left[\frac{1}{L^3}\right]\left\langle\left[\sum_i s_{i\alpha}e^{-i\mathbf{q}\cdot\mathbf{R}_i}\right]^2\right\rangle^{1/2} \tag{25}$$

(where $\alpha=x,y$) were calculated with $\mathbf{q}=0$, $\mathbf{Q}_n(n=1-3)$, given by (7). Quantities were averaged over 2–8 runs using random initial spin configurations. For each run, 10 000 Monte Carlo steps (MCS) per spin were used with the initial 4000 MCS discarded for thermalization.

Boundary lines of the phase diagram shown in Fig. 7 were determined by the behavior of the primary Fourier component $M_{\alpha}\equiv M_{\alpha}(\mathbf{Q}_1)$ for constant H and T scans using a lattice of size $L=12$. Appropriate order parameters for the paramagnetic-linear (1-5A) and linear-elliptical (5A-7) transitions were taken to be M_y and M_x, respectively (see Sec. II). Illustrative data are shown in Figs. 8 and 9, which display behavior typical of second-order phase transitions.[31] The critical temperature (T_c) and fields (H_c) were determined from such results by the location of the points of inflection. These were estimated with the aid of cubic spline fits to the data, giving errors of less than ± 0.02 in T_c and ± 0.2 in H_c. The Néel temperature was found to be $T_N=1.45\pm 0.02$, in agreement with Kawamura.[4] Qualitative similarity between the phase diagrams calculated by these Monte Carlo simulations and by molecular-field theory is evident on comparing Figs. 7 and 3.

Note that in Fig. 7 the paramagnetic-linear phase boundary near T_N rises vertically and then curves to the

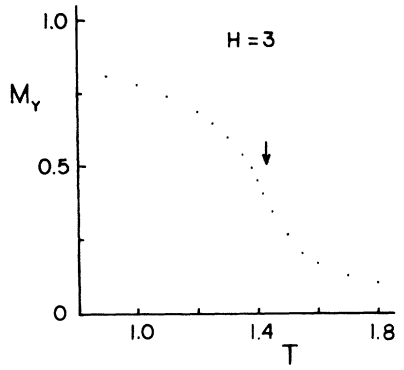

FIG. 8. Temperature dependence of the primary order parameter at $H=3$ for the 1-5A phase transition from Monte Carlo simulations with $L=12$. Arrow indicates estimated critical temperature determined by the point of inflection.

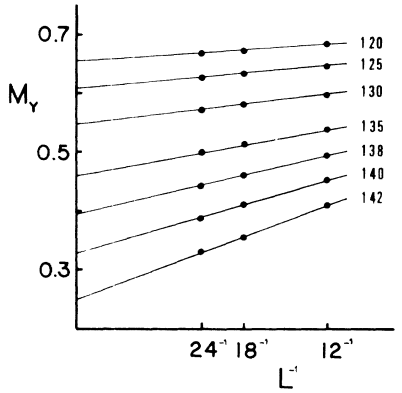

FIG. 10. Finite-size effect on the order parameter at $H=3$ for the 1-5A transition at selected temperatures $T=1.20-1.42$ below the transition $T_c \cong 1.430$.

left, as found in the mean-field results with isotropic ($J_\parallel = J_\perp$: Fig. 3) and strongly anisotropic ($J \gg J_\perp$: Fig. 6) exchange parameters. The Monte Carlo simulations of Mason, Collins, and Gaulin[15] show this boundary curving to the right. All of these results taken together suggest that an increase in T_c of this transition line with increasing field strength is a consequence of effects from both critical fluctuations and the quasi-one-dimensional aspect of the exchange interactions.

The analysis in Ref. 17 of the multicritical point at $T=T_N$ and $H=0$ suggests that the asymptotic behavior of both critical lines is governed by $H^2 \sim |T_N - T|^\phi$ with a crossover exponent $\phi \cong 1.04$. It is clear from the H^2-T plot shown in Fig. 7(b) that the data near T_N fall on nearly straight lines, although a small curvature may be seen in the data for the 1-5A phase boundary. These Monte Carlo simulations thus provide support for the prediction that ϕ is very close to unity. The broken lines of Fig. 7(b) are from the molecular-field relations (22), showing remarkable agreement with the simulation data for the 5A-7 phase boundary.

Finite-size scaling estimates of the critical exponent β were also made for the 1-5A and 5A-7 transitions from temperature scans at $H=3$ and field scans at $T=0.9$, respectively. Data below the transition in each case were analyzed, and for this purpose we adopted the nonstandard method of accounting for L dependence of data, due to spin waves as described by Kawamura.[4] At large L, the spin-wave correction to the staggered magnetization vector of the present system appears as

$$M_\alpha(L) = M_\alpha(\infty) + c_\alpha / L \ . \tag{26}$$

Kawamura notes that this is the dominant finite-size effect if the quantity $x = tL^{1/\nu}$, where $t = (T_N - T)/T_N$, is not large, as is the case with our data. Plots of $M_\alpha(L)$ versus $1/L$ at temperatures $T \lesssim T_N$ then yield $M_\alpha(\infty)$. With β defined by $M_\alpha(\infty) \sim t^\beta$, log-log plots of the temperature dependence of $M_\alpha(\infty)$ then give an estimate of this critical exponent. In this way, Kawamura deduced a value $\beta = 0.25 \pm 0.02$ for the transition at T_N, compared with his earlier result of 0.22 from standard finite-size scaling techniques.

The transition temperature for the paramagnetic-linear phase boundary at $H=3$ is estimated to be $T_c = 1.430 \pm 0.005$. Figure 10 shows the finite-size analysis based on relation (26) at selected temperatures $T < T_c$ for lattices of size $L=12$, 18, and 24. The log-log plot of the resulting data for $M_y(\infty)$ displayed in Fig. 11

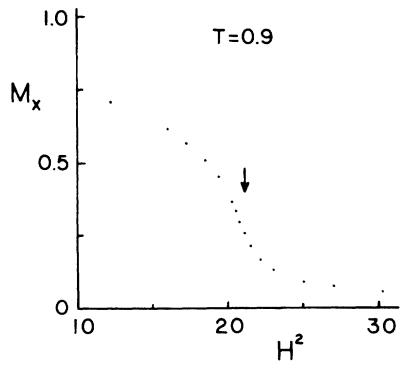

FIG. 9. As in Fig. 8, showing here the H^2 dependence of the primary order parameter at $T=0.9$ for the 5A-7 phase boundary.

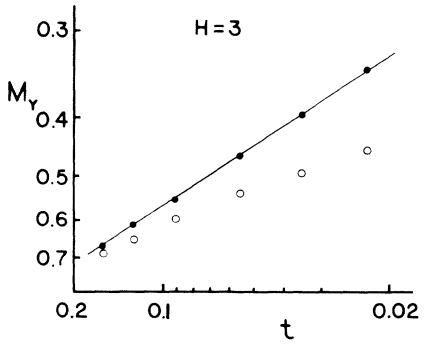

FIG. 11. Log-log plot of the temperature dependence of the order parameter for $H=3$ for the 1-5A transition. Open circles indicate $L=12$ data, and solid circles show the data extrapolated to $L=\infty$ from Fig. 10. Slope of the line gives $\beta \cong 0.34$.

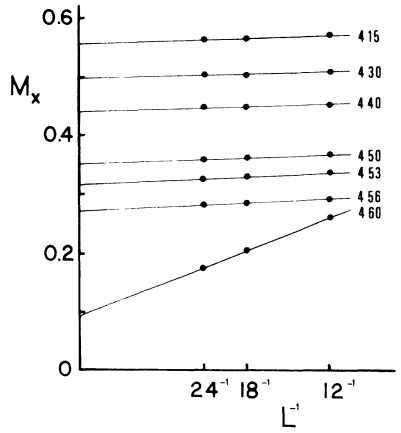

FIG. 12. Finite-size effect on the order parameter at $T=0.9$ for the 5A-7 transition at selected fields $H=4.15-4.60$ below the transition $H_c \cong 4.605$.

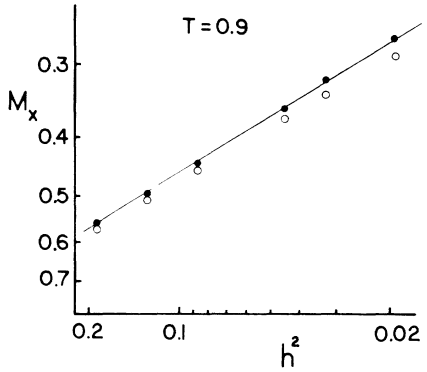

FIG. 13. Log-lot plot of the $h^2=(H_c^2-H^2)/H_c^2$ dependence of the order parameter at $T=0.9$ for the 5A-7 transition. Open circles indicate $L=12$ data, and solid circles show the data extrapolated to $L=\infty$ from Fig. 12. Slope of the line gives $\beta \cong 0.32$

yields the estimate $\beta=0.34\pm0.02$, in agreement with the predicted[17] XY critical behavior (to be compared with, e.g., accurate ε-expansion results $\beta \cong 0.349$ for this universality class[32]).

Finite-size effects for the linear-elliptical transition at $T=0.9$ for selected values of $H<H_c=4.605\pm0.005$ are shown in Fig. 12. These data were analyzed using the relation $M_x \sim (h^2)^\beta$, where $h^2=(H_c^2-H^2)/H_c^2$, as shown in Fig. 13. Field dependence of this form follows from noting that the second-order coefficient $r_0=at$ of standard Landau-Ginzburg-Wilson Hamiltonians takes the renormalized form $r=at+bH^2$ when a magnetic field is applied to an antiferromagnet [see, e.g., the free energy (19)]. The data of Fig. 13 yield the estimate $\beta=0.32\pm0.02$, supporting the prediction that this transition belongs to the Isling universality class (cf. $\beta \cong 0.327$ from Ref. 32). Note from Figs. 10–13 that there is a much smaller finite-size effect for this transition than at the 1-5A phase boundary.

V. CONCLUSIONS

This work has demonstrated a number of new results for magnetic phase diagrams of the planar model on a stacked-triangular lattice with nearest-neighbor antiferromagnetic exchange coupling. The ground-state phase diagram as a function of in-plane applied magnetic field and intraplanar coupling ($J_\perp$) exhibits a rich structure involving an "elliptical" and three types of "linear" ordered states, as characterized by the polarization of the primary wave-vector component $\mathbf{Q}_1=\frac{1}{2}\mathbf{G}_\parallel+\frac{1}{3}\mathbf{G}_\perp$ of the spin density. The stability of the intermediate linear phase (5B) only in a very narrow region of the phase diagram near $J_\parallel=J_\perp$ was shown to be a consequence of the relative weakness of the incidental wave-vector components which distinguish this state from the other two linearly polarized phases.

The Fourier expansion of the spin density provided a convenient description of long-range magnetic order from a Landau-type expansion of the free energy formulated within the molecular-field approximation to examine the structure of (H,T) phase diagrams near T_N. In cases where $J_\perp$ is not too large, splitting of the Néel temperature by the field into two lines of second-order transitions was found, in support of our earlier phenomenological model.[16] Of particular interest is the large-$J_\perp$ case where one of the phase boundaries becomes a line of first-order transitions. This feature suggests that for weak interplane coupling, the criticality of the transition at T_N may not be $n=2$ chiral, as it is for larger $J_\parallel/J_\perp$. Experimental studies on the magnetic phase diagrams of hexagonal materials with planar anisotropy and quasi-two-dimensional exchange coupling, such as[33] $LiCrS_2$, are clearly of interest.

Finally, our Monte Carlo simulations for the case $J_\parallel=J_\perp$ provide support for the recent symmetry, scaling, and renormalization-group analysis[17] on the critical behavior of the $n=2$ chiral multicritical point. This data suggests that the crossover exponent ϕ is close to unity, as calculated by Kawamura, and that the critical exponents β estimated for each of the two phase boundary lines are consistent with the predicted XY and Ising universality.

Note added in proof. Recent Monte Carlo simulations[34] for the case $J_\parallel=1$, $J_\perp=10$ indicate strong critical-fluctuation effects on the magnetic phase diagram (Fig. 5). Tetracritical behavior, as in the isotropic and quasi-one-dimensional cases, is observed. The estimated value for β at $H=0$ is consistent with the $n=2$ chiral universality class.

ACKNOWLEDGMENTS

The authors thank A. Mailhot for useful discussions and programming assistance. This work was supported by Natural Sciences and Engineering Research Council (NSERC) of Canada and Fonds pour la Formation de Chercheurs et L'Aide à la Recherche (FCAR) du Québec. Some of the computing was performed at the Ontario Centre for Large Scale Computation.

[1]R. S. Gekht and V. I. Ponomarev, Phase Transit. **20**, 27 (1990).
[2]H. Kawamura, Phys. Rev. B **38**, 4916 (1988).
[3]H. Kawamura, J. Appl. Phys. **63**, 3086 (1988).
[4]H. Kawamura, J. Phys. Soc. Jpn. **58**, 584 (1989).
[5]H. T. Diep, Phys. Rev. B **39**, 397 (1989).
[6]B. D. Gaulin, M. Hagen, and H. R. Child, J. Phys. (Paris) Colloq. **49**, C8-327 (1988).
[7]T. E. Mason, B. D. Gaulin, and M. F. Collins, Phys. Rev. B **39**, 586 (1989).
[8]B. D. Gaulin, T. E. Mason, M. F. Collins, and J. Z. Larese, Phys. Rev. Lett. **62**, 1380 (1989).
[9]W. E. Murray, Jr., D. P. Belanger, and B. D. Gaulin, Am. Phys. Soc. Bull. **35**, 552 (1990).
[10]D. H. Lee, J. D. Joannopoulos, J. W. Negle, and D. P. Landau, Phys. Rev. Lett. **52**, 433 (1984); Phys. Rev. B **33**, 450 (1986).
[11]H. Kawamura and S. Miyashita, J. Phys. Soc. Jpn. **53**, 4138 (1984); S. Miyashita and H. Kawamura, *ibid.* **54**, 3385 (1985).
[12]B. Schaub and D. Mukamel, Phys. Rev. B **32**, 6385 (1985).
[13]M. L. Plumer, A. Caillé, and K. Hood, Phys. Rev. B **39**, 4489 (1989).
[14]M. Poirier, M. Castonguay, A Caillé, M. L. Plumer, and B. D. Gaulin, Physica B **165**, 171 (1990).
[15]T. E. Mason, M. F. Collins, and B. D. Gaulin, J. Appl. Phys. **67**, 5421 (1990).
[16]M. L. Plumer and A. Caillé, Phys. Rev. B **41**, 2543 (1990).
[17]H. Kawamura, A. Caillé, and M. L. Plumer, Phys. Rev. B **41**, 4416 (1990).
[18]D. H. Lee, R. G. Caflisch, J. D. Joannopoulos, and F. Y. Wu, Phys. Rev. B **29**, 2680 (1984).
[19]H. Kawamura and S. Miyashita, J. Phys. Soc. Jpn. **54**, 4530 (1985).
[20]R. G. Caflisch, Phys. Rev. B **41**, 432 (1990).
[21]A. V. Chubukov, J. Phys. C **21**, L441 (1988).
[22]H. Tanaka, S. Teraoka, E. Kakehasi, K. Iio, and K. Nagata, J. Phys. Soc. Jpn. **57**, 3979 (1988).
[23]A. Mailhot, M. L. Plumer, and A. Caillé, J. Appl. Phys. **67**, 5418 (1990).
[24]The exchange couplings $(J_{\parallel},J_{\perp})$ are defined here as in Ref. 23 and are related to those of Refs. 15 and 21 (J,J') by $J_{\parallel}=2JS^2$ and $J_{\perp}=2J'S^2$.
[25]M. L. Plumer, A. Caillé, and K. Hood, Phys. Rev. B **40**, 4958 (1989).
[26]M. L. Plumer and A. Caillé, Phys. Rev. B **37**, 7712 (1988).
[27]X. Zhu and M. B. Walker, Phys. Rev. B **36**, 3830 (1987).
[28]P. Bak and J. von Boehm, Phys. Rev. B **21**, 5297 (1980).
[29]N. Suzuki, J. Phys. Soc. Jpn. **52**, 3199 (1983).
[30]S. Alexander and P. Pincus, J. Phys. C **13**, 263 (1980).
[31]D. P. Landau and K. Binder, Phys. Rev. B **17**, 2328 (1978).
[32]J. C. Le Guillon and J. Zinn-Justin, J. Phys. (Paris) Lett. **46**, L137 (1985).
[33]B. van Laar and D. J. W. Ijdo, J. Solid State Chem. **3**, 590 (1971).
[34]M. L. Plumer and A. Caillé, J. Appl. Phys. (to be published).